10 Micromagnetic Spin Structure

R. Skomski

Department of Physics and Astronomy and Center for Materials Research and Analysis, University of Nebraska, Lincoln NE 68588, USA

Abstract. Magnetization inhomogenities, associated for example with grain boundaries, give rise to local spin-dependent potentials and affect the magnetoresistance. The local magnetization $\boldsymbol{M}(\boldsymbol{r})$ depends on both intrinsic and extrinsic factors. Intrinsic properties, such as spontaneous magnetization and anisotropy, are determined on an atomic scale and are basically independent of the material's real structure and history. Extrinsic properties, such as remanence and coercivity, are linked to magnetic hysteresis, realized on mesoscopic or macroscopic length scales, and are strongly real-structure dependent. The local magnetization $\boldsymbol{M}(\boldsymbol{r})$, which determines the magnetoresistance, is determined from a nonlinear and nonlocal micromagnetic energy functional containing the intrinsic properties as parameters. This chapter focuses on basic micromagnetic effects and on the spin structure at grain boundaries. Continuum and layer-resolved analytic calculations yield a quasi-discontinuity of the magnetization between misaligned and in-completely exchange-coupled grains and a disproportionally large grain-boundary magnetoresistance.

10.1 Introduction

Electron scattering in advanced magnetoresistive materials depends on the spin-dependent potential associated with the local magnetization $\boldsymbol{M}(\boldsymbol{r})$. In order to abstract from the atomic origin of the magnetoresistance, which is different for GMR [1,2,3,4,5], CMR [6,7,8,9], and PMR materials [10], we introduce the term spin-projecting magnetoresistance (SMR). The basic assumption of SMR is that the magnetoresistance is a unique though generally difficult-to-calculate function of $\boldsymbol{M}(\boldsymbol{r})$. SMR must be distinguished from ordinary magnetoresistance and anisotropic magnetoresistance, which reflect Lorentz forces in typically non-magnetic metals and spin-orbit coupling in transition metals, respectively. Physically, SMR means that the magnetic field alters the mean free paths for $\uparrow$ and $\downarrow$ channels by modifying the local potential felt by the conduction electrons.

The Bloch character of one-electron wave functions in perfect crystals implies zero resistivity, but thermal or structural disorder yield finite mean free paths λ, finite relaxation times τ, and nonzero resistivities $\rho \propto 1/\tau$. Due to the Pauli principle, the interaction between electrons depends on the relative spin orientation, so that the local potential and the electron scattering is spin-dependent (see Chap. 4). Subject to the availability of electronic states – as epitomized by the density of states at the Fermi level – this mechanism leads to an explicit magnetization dependence of the resistivity.

M.J. Thornton and M. Ziese (Eds.): LNP 569, pp. 204–231, 2001.

In the case of weakly inhomogeneous materials the resistivity is proportional to the square of the gradient of the spin-dependent local potential [11] and therefore proportional to the square of the magnetization gradient. Since magnetization inhomogenities are most pronounced in low and moderate magnetic fields $\boldsymbol{H}$, the resistance may be very large at low fields, whereas high magnetic fields reduce the resistance by aligning the spins.

The determination of the local magnetization (mesoscopic spin structure) is a micromagnetic problem. The traditional term micromagnetic [12] is somewhat unfortunate, because most micromagnetic phenomena – such as magnetic hysteresis – are nanostructural, realized on deep-submicron length scales. Micromagnetic or extrinsic properties reflect the *real structure* (defect structure, morphology, metallurgical microstructure) of a material. By contrast, intrinsic properties, such as spontaneous magnetization and magnetocrystalline anisotropy, refer to perfect crystals.

Micromagnetic problems are usually solved on a continuum level [12,13,14]. Narrow-wall phenomena, which have been studied for example in rare-earth cobalt permanent magnets [15], involve individual atoms and atomic planes and lead to comparatively small corrections to the extrinsic behavior. However, in the context of spin electronics, grain-boundary related scattering is generally non-negligible [4,8,9,16,17] and involves quite small length scales of about 1 nm [8]. This may lead to a disproportionally strong spin scattering and calls for a comparison of continuum and layer-resolved calculations.

This chapter elaborates basic ideas of magnetism and, in a sense, considers thin films, paramagnetic gases, bulk magnets, small particles, and wires on an equal footing. Sect. 10.2 is a brief summary of the atomic origin of magnetism, Sect. 10.3 deals with fundamental aspects of micromagnetism, and Sect. 10.4 is devoted to grain-boundary and narrow-wall phenomena.

10.2 Intrinsic Properties

Intrinsic properties refer to the atomic origin of magnetism and involve quantum phenomena such as exchange, crystal-field interaction, interatomic hopping, and spin-orbit coupling [18,19,20,21,22]. Quantities describing the mesoscopic spin structure, such as the coercivity H_c and the remanence M_r, are extrinsic (real-structure related) [14,23,24,25], but intrinsic properties enter micromagnetic equations as local *micromagnetic parameters*. Table 10.1 shows the magnetic moment m, the spontaneous magnetization M_S, the Curie temperature T_C, and first uniaxial anisotropy constant K_1 for some magnetic materials. Not included are antiferromagnets, such as NiO, $GdFeO_3$, and Ti_2O_3, whose long-range magnetic order vanishes above the Néel temperature T_N, and oxides such as CrO_2 (FM), and $Y_3Fe_5O_{12}$ (FIM) (see Chaps. 12 and 6).

10.2.1 Magnetic Moment, Exchange, and Magnetization

Magnetic solids contain atoms characterized by a quantum-mechanical *magnetic dipole moment* $\hat{\mathbf{m}} = -\mu_B(\hat{\mathbf{l}} + 2\hat{\mathbf{s}})/\hbar$. Often one considers the net magnetic mo-

Table 10.1. Intrinsic and structural properties of some magnetic materials (FM = ferromagnet, FIM = ferrimagnet).

	m	$\mu_0 M_S$	T_C	K_1	Comment
	μ_B/f.u.	T	K	MJ/m^3	
Fe	2.23	2.15	1044	0.05	Cubic FM
Co	1.73	1.81	1390	0.53	Hexagonal FM
Ni	0.62	0.62	628	-0.005	Cubic FM
$SmCo_5$	8.0	1.07	1020	17.2	Hexagonal FM
$Nd_2Fe_{14}B$	37.6	1.61	585	4.9	Tetragonal FM
$BaFe_{12}O_{19}$	19.9	0.47	742	0.33	Hexagonal FIM
Fe_3O_4	4.0	0.63	860	-0.012	Cubic FIM

ment m per formula unit, which is measured in μ_B. An alternative way of characterizing a material's net moment is to consider the spontaneous *magnetization* $M_S = dm/dV$, measured in A/m, or its flux-density equivalent $\mu_0 M_S$, measured in T. Here dV is a small volume element containing at least one unit cell. Since thermal excitations tend to disalign the atomic moments, the spontaneous magnetization is temperature-dependent. The zero-temperature spontaneous magnetization $M_S(T = 0)$ is determined by the atomic moments and often denoted by M_0.

There are two sources of magnetic moment: currents associated with the orbital motion of the electrons (orbital moment) and the electron spin (spin moment). Solid-state magnetism originates from the partly filled inner electron shells of transition-metal atoms. Of particular importance are the $3d$ iron-series elements, in particular Fe, Co, and Ni, and the $4f$ rare-earth elements, such as Nd, Sm, Gd, and Dy. On the other hand, $4d$ palladium-series elements, $5d$ platinum-series elements, and actinide elements, such as U, have a magnetic moment in suitable crystalline environments.

The magnetic moment of iron-series transition-metal atoms in metals (Fe, Co, Ni, YCo_5) and non-metals (Fe_3O_4, NiO) is given by the *spin*, so that the moment, measured in μ_B, is equal to the number of unpaired spins. The reason is that the orbital moment is largely quenched (destroyed) by the crystal field, although the small residual orbital moment (of the order of $0.1\mu_B$) is important in the context of magnetic anisotropy. Rare-earth atoms keep their orbital moments in metals and non-metals, because their partly filled shells lie deep inside the atoms and are not very much affected by the crystal field.

Figure 10.1 illustrates that the net magnetic moment depends on the type of zero-temperature magnetic order. In ferromagnets the atomic moments add, whereas ferrimagnets and antiferromagnets are characterized by two (or more)

sublattices with opposite moments. This amounts to a reduction of the net moment (ferrimagnetism) or to the absence of a net moment (antiferromagnetism).

In order to understand moment formation and magnetic order one has to start from the many-electron Schrödinger equation (see Chaps. 2 and 5). The solution of that equation is complicated by Coulomb interactions of the type $1/|\boldsymbol{r} - \boldsymbol{r}'|$, where $\boldsymbol{r}$ and $\boldsymbol{r}'$ are the positions of the interacting electrons. For non-interacting electrons, the many-electron wave function factorizes, but the Coulomb repulsion makes such a separation impossible and gives rise to a variety of intra- and interatomic exchange contributions.

In the case of two electrons and two atomic sites, the problem reduces to the discussion of three parameters: the *hopping parameter* t, the *Coulomb* energy U necessary to add a second electron into an atomic orbital, and the *direct exchange* J_D [14]. The direct exchange is always positive, but for interatomic distances of interest it is not larger than about 0.1 eV, that is smaller than U and t by at least one order of magnitude. Comparing the energies of the lowest-lying $\uparrow\uparrow$ and $\uparrow\downarrow$ states yields the *effective exchange*

$$J_\mathrm{eff} = J_\mathrm{D} + \frac{U}{4} - \sqrt{t^2 + \frac{U^2}{16}} \tag{10.1}$$

From this equation we see that the Coulomb repulsion U and the direct exchange J_D favor ferromagnetism ($J_\mathrm{eff} > 0$), whereas interatomic hopping (t) tends to destroy ferromagnetism. The reason is that $\uparrow\downarrow$ electron pairs in an atomic orbital are unfavorable from the point of view of Coulomb repulsion, whereas parallel spin alignment $\uparrow\uparrow$ is favorable, because the Pauli principle implies that the two electrons are in different orbitals. However, this energy gain has to compete against a hopping-related increase in one-electron energies.

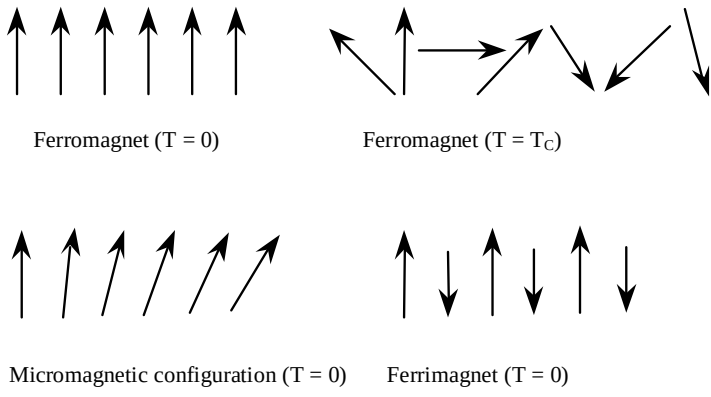

Fig. 10.1. Magnetic order (schematic). Magnetoresistance involves both zero-temperature and finite temperature magnetic ordering. Much of the fascination of advanced magnetoresistive phenomena is based on the intriguing interplay between microscopic and mesoscopic physics (micromagnetism).

In oxides, $t \ll U$ and (10.1) yields $J_{\rm eff} = J_{\rm D} - 2t^2/U$. Due to the smallness of the direct exchange, oxides are often antiferromagnets, but when $t = 0$ by symmetry, as in CrO_2, then $J_{\rm D}$ gives rise to ferromagnetism (Goodenough-Kanamori rules, see Chaps. 5 and 12). In $3d$ metals, $t \gg U$ and (10.1) yields $J_{\rm eff} = J_{\rm D} + U/4 - t$. Since U is a largely atomic property, metallic ferromagnetism is realized for not-too-large hopping, that is for narrow bands (Stoner criterion, see Chap. 2).

In order to discuss magnetic order, it is necessary to distinguish between intra-atomic and interatomic exchange interactions. Intra-atomic exchange is responsible for the formation of atomic moments, whereas interatomic exchange favors a ferromagnetic (or antiferromagnetic) alignment of neighboring spins. Typically, the intra-atomic exchange $J_{\rm intra}$ is much larger than the interatomic exchange $J_{\rm inter} = J$, and atomic moments tend to be quite stable. By comparison, it is comparatively easy to disalign neighboring spins by thermal excitation and – to a lesser extent – by inhomogeneous magnetic fields and polycrystalline random-anisotropy contributions.

A widely-used approach to discuss interatomic exchange is the *Heisenberg* interaction $-J\hat{\mathbf{s}}_1 \cdot \hat{\mathbf{s}}_2$ between neighboring spins $\hat{\mathbf{s}}_1$ and $\hat{\mathbf{s}}_2$, where J is an interatomic exchange constant. The derivation of the spontaneous magnetization $M_{\rm S}$ of a solid from the corresponding Heisenberg Hamiltonian is a very complicated problem, but a number of approximations (normalized classical spins, restriction to nearest-neighbor interactions, mean-field approximation) lead to the simple result that $M_{\rm S}$ vanishes above the *Curie temperature* $T_{\rm C} = zJ/3{\rm k_B}$, where z is the number of nearest neighbors.

Strictly speaking, the applicability of the Heisenberg model is limited to local-moment magnets, such as insulating transition-metal oxides and rare-earth metals. In $3d$ metals, the magnetic moment is a band-structure property, involving at least a few neighboring atoms [14,26]. This leads to non-integer moments per atom, may yield moment and exchange-constant corrections at grain boundaries and interfaces, and means that quantities such as J and m should be considered as atomic parameters.

As indicated in Fig. 10.1, the vanishing of the spontaneous magnetization at $T_{\rm C}$ reflects the thermally activated rotational misalignment of the atomic moments. By contrast, the magnitude of the atomic moments remains largely unchanged [27]. The reason is that atomic moments are supported by intra-atomic exchange energies of the order of 1 eV (10^4 K), whereas the interatomic exchange does not exceed about 0.1 eV. This scenario is realized in both metals and nonmetals, although interatomic hopping in itinerant metals, such as iron, may yield short-range correlations at and above $T_{\rm C}$. The magnetization $M_{\rm S}$ considered in micromagnetism is usually *averaged* over a few interatomic distances and can be regarded as a temperature-dependent but field-independent material constant (micromagnetic parameter). This means, in particular, that micromagnetic phenomena, such as domain formation and hysteresis, are realized by magnetization *rotations*.

Aside from long-range critical fluctuations in the vicinity of T_C, the spontaneous magnetization is caused by atomic-scale exchange interactions. However, there is also an exchange energy associated with micromagnetic magnetization rotations, such as domains. The local magnetization can be written as $\boldsymbol{M}(\boldsymbol{r}) = M_S(T)\boldsymbol{s}(\boldsymbol{r})$, where $\boldsymbol{s}(\boldsymbol{r})$ is the unit vector giving the local magnetization direction. Heisenberg exchange means that spin misalignment in ferromagnets ($J > 0$) costs exchange energy. On a continuum level, the normalized magnetization $\boldsymbol{s}_{1/2} = \boldsymbol{s}(\boldsymbol{r}) \pm b\,\partial\boldsymbol{s}(\boldsymbol{r})/\partial x$ of two neighbouring atoms located at $\boldsymbol{r}_{1/2} = \pm b\boldsymbol{e}_x$ correspond to the exchange energy

$$-J\boldsymbol{s}_1 \cdot \boldsymbol{s}_2 = -J + Jb^2 \left(\frac{\partial \boldsymbol{s}}{\partial x}\right)^2 \tag{10.2}$$

More generally, any magnetization inhomogenity is punished by an exchange energy density

$$\frac{\mathrm{d}E_{\mathrm{ex}}}{\mathrm{d}V} = A\,(\nabla \boldsymbol{s})^2 \tag{10.3}$$

where the *exchange stiffness* A is of the order of 10 pJ/m (10^{-11} J/m) for typical ferromagnets, see Table 10.2.

10.2.2 Anisotropy

The energy of a magnetic solid depends on the orientation of the magnetization with respect to the crystal axes, which is known as magnetic *anisotropy*. The anisotropy of permanent magnets is high in order to keep the magnetization in a desired direction, whereas soft magnets are characterized by a very low anisotropy. Materials with moderate anisotropy are often used as magnetic-recording media. In the field of magnetoresistance, anisotropy is a double-edged issue: high anisotropies enhance the magnetization gradient and the magnetoresistance, but they also make the material more difficult to magnetize.

It is convenient to write the magnetization as

$$\boldsymbol{M} = M_S\left[\sin(\theta)\sin(\varphi)\boldsymbol{e}_x + \sin(\theta)\cos(\varphi)\boldsymbol{e}_y + \cos(\theta)\boldsymbol{e}_z\right]. \tag{10.4}$$

The simplest anisotropy-energy expression is then

$$E_a = K_1 V \sin^2(\theta), \tag{10.5}$$

where K_1 is the *first uniaxial anisotropy constant* and V is the magnet volume [28]. Equation (10.5) is widely used to describe uniaxial magnets (hexagonal, tetragonal, and rhombohedral crystals) and small ellipsoids of revolution (fine particles). For $K_1 > 0$ the easy magnetic direction is along the c- (or z-) axis, which is called *easy-axis anisotropy*, whereas $K_1 < 0$ leads to *easy-plane anisotropy*, where the easy magnetic direction is anywhere in the a-b- (or x-y-) plane. In cubic magnets there is no unique z-axis, but (10.5) can be used for

small angles θ (see below). For very low symmetry (orthorhombic, monoclinic, and triclinic), the first-order anisotropy energy can be written as

$$E_\mathrm{a} = K_1 V \sin^2(\theta) + K_1' V \sin^2(\theta)\cos(2\varphi)\,, \tag{10.6}$$

where K_1 and K_1' are, in general, of comparable magnitude. This expression must also be used for magnets having a low-symmetry shape, such as ellipsoids having three unequal principal axes, and for a variety of surface anisotropies, such as that of bcc (011) surfaces.

An expression including second order anisotropy constants is [28]

$$\frac{E_\mathrm{a}}{V} = K_1 \sin^2(\theta) + K_2 \sin^4(\theta) + K_2' \sin^4(\theta)\cos(4\varphi)\,. \tag{10.7}$$

This equation describes tetragonal, hexagonal, rhombohedral and cubic crystals. Hexagonal and rhombohedral crystals are characterized by $K_2' = 0$ (fourth-order uniaxial anisotropy), whereas in the tetragonal case K_2 and K_2' are of the same order of magnitude.

The anisotropy of cubic crystals is often written as

$$\frac{E_\mathrm{a}}{V} = K_1^\mathrm{c}\left(\alpha_1^2\alpha_2^2 + \alpha_2^2\alpha_3^2 + \alpha_3^2\alpha_1^2\right) + K_2^\mathrm{c}\,\alpha_1^2\alpha_2^2\alpha_3^2\,, \tag{10.8}$$

where $\alpha_1 = \cos(\theta)$, $\alpha_2 = \sin(\theta)\cos(\varphi)$, and $\alpha_3 = \sin(\theta)\sin(\varphi)$ are the direction cosines of the magnetization direction. Analysis of (10.8) shows that $K_1^\mathrm{c} > 0$ favors the alignment of the magnetization along the (001) cube edges, which is called iron-type anisotropy, whereas $K_1^\mathrm{c} < 0$ corresponds to an alignment along the (111) cube diagonals referred to as nickel-type anisotropy. Comparison of (10.7) and (10.8) yields $K_2 = -7K_1^\mathrm{c}/8 + K_2^\mathrm{c}/8$ and $K_2' = -K_1^\mathrm{c}/8 - K_2^\mathrm{c}/8$. These relations mean (i) that the constant K_1 in cubic materials reflects fourth-order crystal-field interactions [14] and (ii) that there are only two independent constants when (10.7) is applied to cubic magnets [14]. Typical K_2^c values are 0.015, 0.05, and 0.28 MJ/m^3 for Fe, Ni, and Fe_3O_4, respectively.

By definition, there are no odd-order terms in (10.6)–(10.8). Odd-order anisotropies may be caused by relativistic Moriya-Dzialoshinskii interactions, exchange biasing, or particular micromagnetic regimes [14,29]. This refers in particular to uni-*directional* anisotropies of the type $K_\mathrm{ud}\cos(\theta)$, which correspond to a hysteresis-loop shift.

With respect to the *physical origin of anisotropy* it is necessary to distinguish between magnetostatic and magnetoelectric anisotropies. Magnetostatic interactions give rise to shape anisotropy, which is illustrated in Fig. 10.2: the magnetostatic energy of the spin configuration (a) is lower than that of the configuration (b), so that the easy magnetization corresponds to the lowest magnetostatic energy. For fine particles (see below), the shape-anisotropy contribution to K_1 is

$$K_\mathrm{1,sh} = \frac{\mu_0}{4}\,(1 - 3N)\,M_\mathrm{S}^2\,, \tag{10.9}$$

where N is the demagnetizing factor of the particle ($N = 0$ for long cylinders, $N = 1/3$ for spheres, and $N = 1$ for plates). Note that (10.9) and the simplified

picture Fig. 10.2 do not apply to large particles, where the exchange stiffness A is not able to ensure a uniform (coherent) spin orientation throughout the magnet (Sect. 10.3.3).

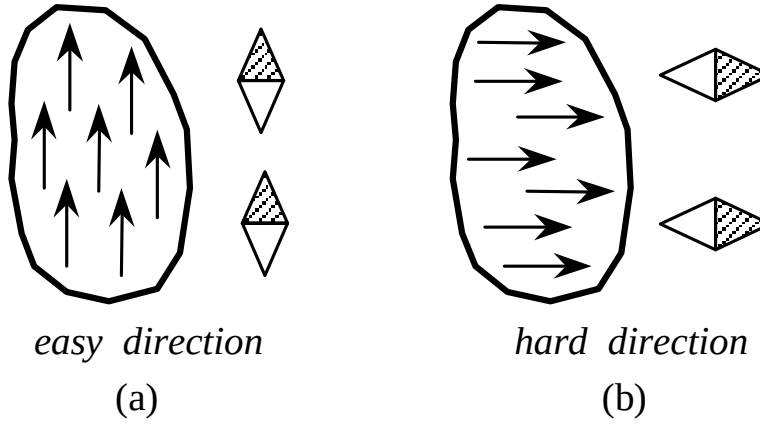

Fig. 10.2. Shape anisotropy of cubic magnets (schematic). The configuration (a) is energetically more favorable than the configuration (b), as one can deduce from the compass-needle analogy.

In non-cubic magnets there is also a magnetostatic contribution to the bulk anisotropy. However, in most materials the bulk or *magnetocrystalline* anisotropy reflects the competition between the spin-orbit coupling and the electrostatic crystal-field interaction (magnetoelectric anisotropy) [30]. The crystal field reflects the local symmetry of the crystal and acts on the orbits of the electrons in the partly filled inner shells. The anisotropy is then realized by the coupling of the orbital moments to the spins by the relativistic spin-orbit coupling $H_{\mathrm{SO}} = \lambda_{\mathrm{SO}} \hat{\mathbf{l}} \cdot \hat{\mathbf{s}}$. The spin-orbit coupling has two consequences: (i) it couples the magnetization (the spin) to the orbital motion of the electrons and (ii) it creates a small orbital moment in largely quenched magnets. Quenched wave functions correspond to standing waves of the type $\cos(2\varphi)$ and are favorable from the point of view of electrostatic crystal-field interaction, because they are able to adapt to the crystal field, but due to the standing-wave character of the quenched wave function the orbital moment and the anisotropy are zero. By contrast, unquenched wave functions, such as $\exp(2\mathrm{i}\varphi)$, do not split in the crystal field benefit from the spin-orbit coupling, because their running-wave character amounts to a circular current.

Depending on the relative strengths of the crystal-field and spin-orbit interactions there are two limits of interest. Rare-earth $4f$ electrons are close to the atomic core and exhibit a strong spin-orbit coupling, whereas the crystal field felt by the $4f$ electrons is rather small. This means a rigid coupling between spin

and orbital moment, and the magnetocrystalline anisotropy is given by the electrostatic interaction of the generally aspherical $4f$ charge cloud with the crystal field [14]. Although the $4f$ crystal field is much smaller than the crystal-field acting on iron-series $3d$ electrons, it creates a high rare-earth anisotropy contribution (Table 10.1). The much smaller anisotropy of $3d$ magnets is explained by the quenching of the orbital moment due to the crystal field. In the limit of complete quenching, $\langle\hat{\mathbf{l}}\rangle = 0$ and $K_1 = 0$, but in reality the weak $3d$ spin-orbit coupling acts as a perturbation and yields some admixture of running-wave character, a small residual orbital moment, and some anisotropy.

In order to illustrate the origin of the $3d$ anisotropy we consider two d orbitals, such as $|\Psi_1\rangle = |xy\rangle$ and $|\Psi_2\rangle = |x^2 - y^2\rangle$. The Hamiltonian is

$$H = \begin{pmatrix} A_0 & 0 \\ 0 & -A_0 \end{pmatrix} + 2\lambda_{\mathrm{SO}} \cos(\theta) \begin{pmatrix} 0 & \mathrm{i} \\ -\mathrm{i} & 0 \end{pmatrix} , \tag{10.10}$$

where the crystal-field parameter A_0 describes the electrostatic energy of the two orbitals in the crystal field, $\cos(\theta)$ is the angle between spin direction and z-axis and the factor 2 is the magnetic quantum number of the d orbitals. Diagonalization of (10.10) yields the energy eigenvalues

$$E_{\pm} = \pm\sqrt{A_0^2 + 4\lambda_{\mathrm{SO}}^2 \cos^2(\theta)}\,. \tag{10.11}$$

By expanding E_- into powers of the small quantity λ_{SO}^2/A_0^2 we obtain the second-order anisotropy energy

$$E_{\mathrm{a}} = \frac{2\lambda_{SO}^2}{A_0} \sin^2(\theta)\,. \tag{10.12}$$

An equation of this type was first derived by Bloch and Gentile [30]. The corresponding orbital moment scales as $\lambda_{\mathrm{SO}}\mu_{\mathrm{B}}/A_0$ [14]. Note that the qualitative result (10.12) applies to both metallic and non-metallic $3d$ magnets, but in metals the crystal-field splitting must be replaced by the band width [21]. To make quantitative predictions one has to extend (10.10) by including all occupied $3d$ orbitals and all unperturbed crystal-field or band-structure states.

The magnetocrystalline anisotropy is closely related to the *magnetoelastic* anisotropy, because strained crystals can be regarded as unstrained crystals having slightly different atomic positions. Magnetoelastic anisotropy is particularly important in cubic magnets, where uniaxial stress gives rise to uniaxial anisotropy contributions. The magnetoelastic contribution to the first anisotropy constant is (see e.g. [14])

$$K_{1,\mathrm{me}} = \frac{3\lambda_{\mathrm{S}}\sigma}{2}\,, \tag{10.13}$$

where σ is the uniaxial stress and λ_{S} is the saturation magnetostriction. Experimental room-temperature values of λ_{S} are -7×10^{-6} for iron, -33×10^{-6} for nickel, 40×10^{-6} for Fe_3O_4, -1560×10^{-6} for $SmFe_2$, 75×10^{-6} for FeCo, and practically zero for $Fe_{20}Ni_{80}$ (permalloy).

As the spontaneous magnetization, anisotropy constants are temperature dependent: atomic excitations lead to the occupation of excited levels, and in the limit of very high temperatures all levels are occupied with equal probability (zero anisotropy). Note that the temperature equivalent of anisotropy energies per atom does not exceed about 1 K, but the switching of individual spins into states with reduced anisotropy is largely suppressed by the strong inter-atomic exchange.

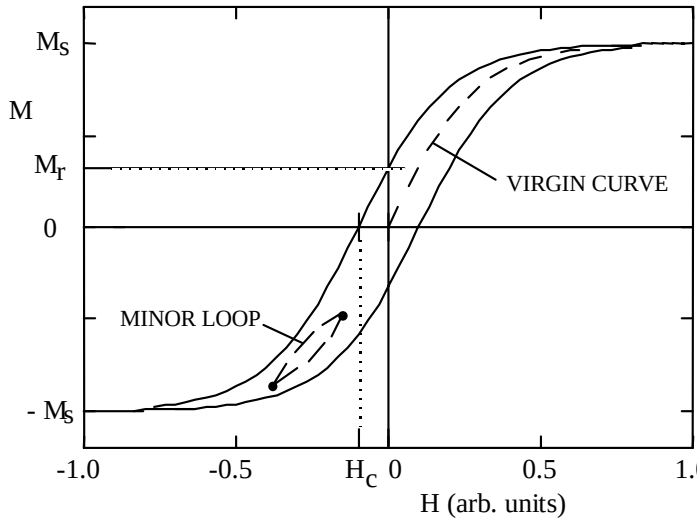

Fig. 10.3. Typical major M-H hysteresis loop.

10.3 Basic Micromagnetism

As mentioned in the introduction, magnetic properties derived from the hysteresis loop are *extrinsic* properties, because they describe the real structure of the magnet rather than the atomic (intrinsic) behavior. Figure 10.3 shows a typical *M-H* hysteresis loop. Note that hysteresis loops are usually corrected for the demagnetizing field $-NM$ by plotting the magnetization as a function of the internal field $H - NM$. In general, this skewing (shearing) correction makes the hysteresis loops more rectangular. *Major* or limiting hysteresis loops are obtained by starting from a fully aligned magnet where $\boldsymbol{M}(\boldsymbol{r}) = M_{\mathrm{S}}\boldsymbol{e}$. This is achieved by applying a large positive field. The loop is then obtained by monitoring the volume-averaged magnetization as a function of the external magnetic field H. *Minor loops* are obtained if the maximum applied field $\pm H$ is insufficient for complete saturation. They lie inside the major loop and therefore include a smaller area than the major loop. *Virgin curves* (initial curves) are obtained on increasing H from zero after thermal demagnetization, that is after heating

beyond T_C. B-H hysteresis loops are used, for example, to determine the energy product of permanent magnets [14].

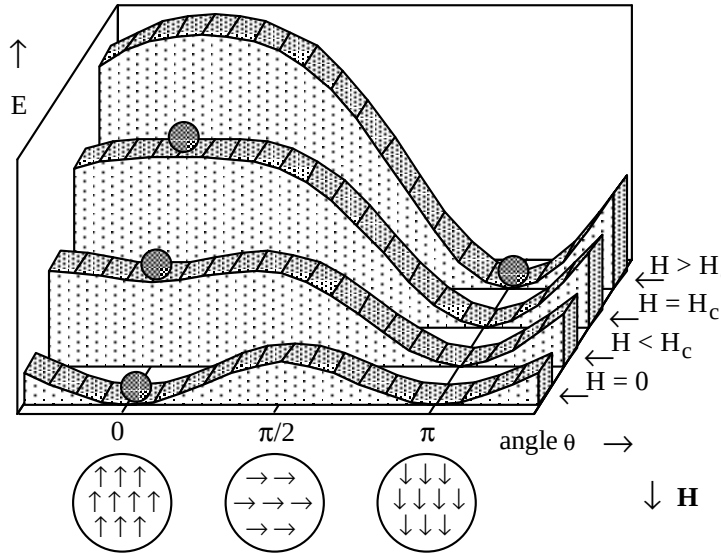

Fig. 10.4. Origin of coercivity: hysteresis involves metastable energy minima.

The most important extrinsic properties are the remanent magnetization or *remanence* M_r which remains in a magnet after switching off a large magnetic field and the coercive force or *coercivity* H_c that is the reverse field at which the average magnetization vanishes. Coercivity describes the stability of the remanent state and gives rise to the classification of magnets into hard magnetic materials (permanent magnets), semi-hard materials (storage media), and soft magnetic materials. Modern permanent magnets exhibit broad hysteresis loops with coercivities of order 1 T (0.8 MA/m), whereas semi-hard materials used in storage media exhibit narrow but rectangular hysteresis loops having coercivities of the order 0.05 T (40 kA/m). The coercivity of storage media is sufficient to assure the remanence of the stored information without requiring powerful and bulky writing facilities. Other extrinsic properties, such as the permanent-magnet energy product and loop squareness, go beyond the exclusive consideration of M_r and H_c. The strong real-structure dependence of extrinsic properties is seen, for example, from the fact that the coercivity of technical iron doubles by adding 0.01 wt.% nitrogen [25]. The reason is that the interstitial nitrogen yields a local modification of K_1 which has a disproportionally strong impact on the motion of domain walls.

The explanation and determination of extrinsic properties is generally very complicated, and only in a few cases it is possible to use simple hysteresis mod-

els. One example is the coherent-rotation or Stoner–Wohlfarth model, which describes the hysteretic behavior of a uniformly magnetized particle (Fig. 10.4). However, truly one-dimensional energy landscapes, such as $E(\theta)$ in Fig. 10.4, are rarely encountered in practice. Most magnetization processes of interest are *incoherent*, and the associated energy landscape is multidimensional. For example, the applicability of the Stoner–Wohlfarth theory is limited to very small particles, and even in the case of single-domain particles (Sect. 10.3.3) the magnetization reversal may be incoherent. A further complication is that the involved micromagnetic equations are nonlocal and nonlinear, and only in a few cases it has been possible to obtain physically transparent solutions.

10.3.1 Coherent Rotation

The *Stoner–Wohlfarth* model [31] assumes that the magnetization remains coherent (uniform) throughout the magnet, as in Figs. 10.2 and 10.4. This is justified for very small particles or very thin films or wires, where the interatomic exchange is able to keep the spins parallel throughout the magnet (see Sect. 10.3.3).

Incorporating the shape anisotropy into K_1, the magnetic energy of an aligned uniaxial Stoner–Wohlfarth particle is

$$\frac{E}{V} = K_1 \sin^2(\theta) + K_2 \sin^4(\theta) - \mu_0 M_S H \cos(\theta)\,, \tag{10.14}$$

where H is the external magnetic field, applied in the z-direction, and $M_z = M_\mathrm{S}\cos(\theta)$. The last term in this equation is the *Zeeman energy* $-\mu_0\, \boldsymbol{m} \cdot \boldsymbol{H}$, which describes the interaction of a magnetized body with the external field.

Putting $H = 0$ in (10.14) yields a variety of zero-field spin configurations. When both K_1 and K_2 are positive, then minimization of (10.14) yields easy-axis anisotropy ($\theta = 0$). On the other hand, when both K_1 and K_2 are negative, then the magnetization lies in the basal plane: easy-plane anisotropy, $\Theta = \pi/2$. A particularly interesting regime is the *easy-cone* magnetism occurring if the conditions $K_1 < 0$ and $K_2 > -K_1/2$ are satisfied simultaneously [14,29]. The tilt angle between the z-axis and the easy magnetization direction is given by

$$\theta_c = \arcsin\left(\sqrt{\frac{|K_1|}{2K_2}}\right)\,. \tag{10.15}$$

Since the temperature dependences of K_1 and K_2 are generally different (K_2 is often negligible at high temperatures), the preferential magnetization direction may change upon heating (spin-reorientation transition). A similar film-thickness dependent transition is observed in films where surface and bulk anisotropy contributions compete.

For $K_2 = 0$, stability analysis of (10.14) yields the coherent-rotation *nucleation field*

$$H_\mathrm{N} = \frac{2K_1}{\mu_0 M_\mathrm{S}} \tag{10.16}$$

at which the $\theta = 0$ state ($M_z = M_S$) becomes unstable. In terms of Fig. 10.4, this instability refers to the vanishing of the local energy minimum at $H_c = H_N$ and leads to a rectangular hysteresis loop.

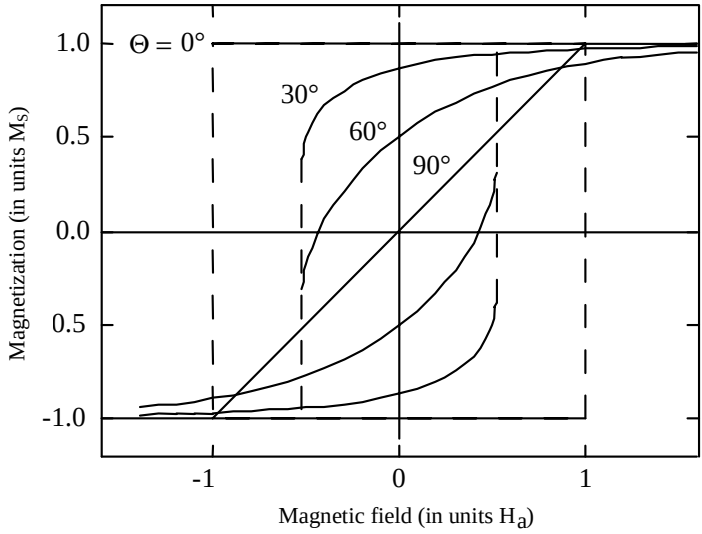

Fig. 10.5. Dependence of the magnetization on the angle θ between field and easy axis for a uniaxial magnet. Dashed lines indicate magnetization jumps.

Equation (10.16) translates the anisotropy constant K_1 into a field quantity, namely the *anisotropy field* $H_a = H_N$. It may be used as a coercivity estimate, although it almost invariably overestimates the coercivity by one order of magnitude. This discrepancy, known as Brown's paradox, is explained by the prevalence of incoherent magnetization processes in real magnets. For anisotropy fields in more complicated magnets see Ref. [14].

Many materials of interest in spin electronics are polycrystallites (nanocrystallites) or powders. Ignoring interparticle interactions, which are discussed in the following sections, we can describe those materials as ensembles of Stoner–Wohlfarth particles, characterized by a coherent rotation of the magnetization. Figure 10.5 shows hysteresis loops of uniaxial Stoner–Wohlfarth particles for different angles θ between the applied magnetic field and the crystallite's c-axis. The magnetic behavior of the material is then obtained as a superposition of Stoner–Wohlfarth loops. For uniaxial magnets the resulting remanence $M_r = M_S/2$, whereas for iron-type ($K_1 > 0$) and nickel-type ($K_1 < 0$) cubic magnets, M_r/M_S equals 0.832 and 0.866, respectively. In the case of uniaxial magnets, the coercivity is equal to $0.479H_a$.

10.3.2 Domains and Domain Walls

Until now we have neglected the mutual magnetostatic dipole interaction between atomic moments. The magnetostatic dipole field created by a magnet's own magnetization is given by

$$\boldsymbol{H}_{\mathrm{d}}(\boldsymbol{r}) = \frac{1}{4\pi} \int \mathrm{d}V' \, \frac{3(\boldsymbol{r}-\boldsymbol{r}')(\boldsymbol{r}-\boldsymbol{r}')\cdot\boldsymbol{M}(\boldsymbol{r}') - |\boldsymbol{r}-\boldsymbol{r}'|^2 \boldsymbol{M}(\boldsymbol{r}')}{|\boldsymbol{r}-\boldsymbol{r}'|^5} \,. \qquad (10.17)$$

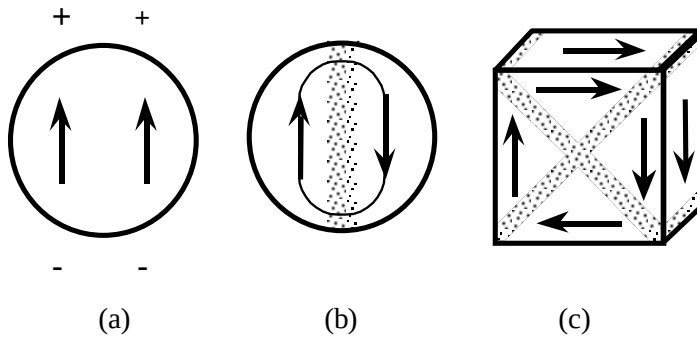

Fig. 10.6. Magnetostatic self-energy and flux closure (schematic). As implied by (10.17), the spin configurations (b) and (c) are more favorable than the configuration (a). The transition between domains is realized by a domain wall (grey area).

Due to a self-interaction contribution, this field differs by $\boldsymbol{M}/3$ from the internal magnetostatic field obtained from Maxwell's equations. However, magnetic fields couple as $\boldsymbol{M}\cdot\boldsymbol{H}$ to the magnetization, so that any term proportional to $\boldsymbol{M}\cdot\boldsymbol{M} = M_{\mathrm{S}}^2$ amounts to a physically irrelevant shift of the zero-point of the self-interaction energy $-(1/2)\mu_0 \int \boldsymbol{H}_{\mathrm{d}}\cdot\boldsymbol{M}\mathrm{d}V$ [32], and the physics of magnetostatic self-interaction is fully contained in (10.17).

By expressing (10.17) in terms of the magnetic charge density $-\nabla\cdot\boldsymbol{M}$ it can be shown that the magnetostatic self-interaction energy is particularly low when there are no magnetic charges at the magnet's surface. From Fig. 10.6 we see that the absence of surface charges is linked to flux closure in the magnet. More generally, magnetostatic interactions tend to yield magnetic *domains* of opposite magnetization directions [23,24,33,34]. This explains why the net magnetization $\langle\boldsymbol{M}(\boldsymbol{r})\rangle$ of many magnets is equal to zero, despite $\boldsymbol{M}(\boldsymbol{r})^2 = M_{\mathrm{S}}^2$ throughout the magnet. For example, two pieces of soft iron do not attract each other, and to exert a force on a soft magnet one needs to destroy the domains by an external field. There are many different domain patterns of interest in the context of magnetoresistance (see particularly Chaps. 14 and 15).

A common feature of all domain structures is that the domains are separated by comparatively sharp *domain walls* [23,24]. The reason for the formation of

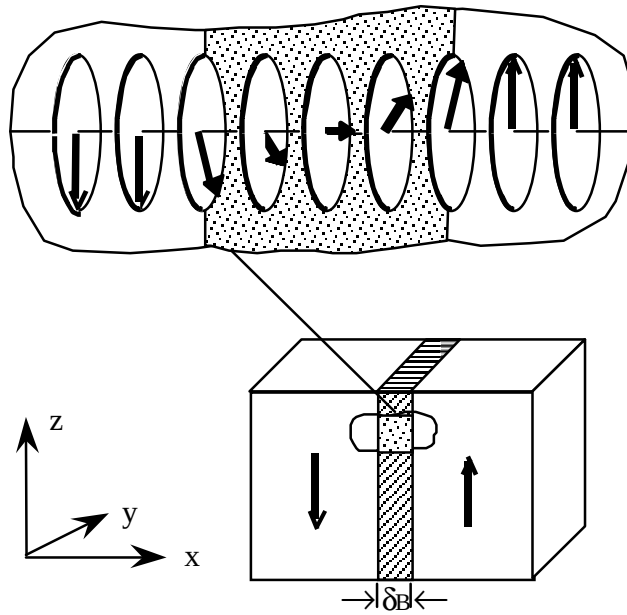

Fig. 10.7. Bloch wall lying in the y-z-plane (schematic). The arrows show the local magnetization direction.

domain walls is that the magnetization inside the domains lies along easy directions, whereas the transition between two easy magnetization directions involves energetically unfavorable spin orientations. Magnetocrystalline anisotropy favors narrow domain walls, but (10.5) shows that narrow walls, that is large magnetization gradients, are unfavorable from the point of view of exchange.

The domain-wall width is estimated very easily from dimensional arguments [23]. The domain-wall width is determined by the anisotropy constant K_1 and the exchange stiffness A, which are measured in J/m^3 and J/m, respectively, so that the only length and the only wall energy derivable from these parameters are the wall-width parameter $\delta_0 = (A/K_1)^{1/2}$ and the wall-energy parameter $\gamma_0 = (K_1 A)^{1/2}$, respectively. This means that the domain-wall thickness tends to be much larger than the interatomic spacing but is much smaller than typical domain sizes.

In order to make quantitative predictions one has to consider specific wall geometries. Figure 10.7 shows a K_1-only Bloch wall, where the *wall thickness* $\delta = \pi\delta_0$ and the wall energy $\gamma = 4\gamma_0$ [14,35]. The 180° Bloch wall shown in Fig. 10.7 is frequently encountered in uniaxial magnets. Other important wall configurations are thin-film 180° Néel walls, where the magnetization vector remains in a plane (in the z-x-plane in Fig. 10.7), and 90° walls observed in cubic crystals. Typical domain-wall widths are 5 nm and 100 nm for hard and soft magnetic materials, respectively.

The magnetostatic dipole interaction favors domain formation, but since the creation of domain walls costs energy, there are no walls if the gain in magnetostatic energy is smaller than the wall energy. For example, the wall in Fig. 10.7b – indicated by the dotted line – corresponds to a wall energy $\gamma\pi R^2$. The competing gain in magnetostatic energy is roughly equal to half the single-domain energy, that is $\mu_0 M_\mathrm{S}^2 V/12$, so that domain formation is favorable for particles whose radius exceeds a *critical single-domain radius*

$$R_\mathrm{sd} \simeq \frac{36\sqrt{AK_1}}{\mu_0 M_\mathrm{S}^2}\,. \tag{10.18}$$

This value varies between a few nm in soft magnets and about 1 μm in hard magnets.

It is important to note that the critical single-domain radius is an equilibrium property and therefore largely unrelated to hysteresis. As illustrated in Fig. 10.4, hysteresis involves energy barriers and metastable states, and in hard magnetic materials, where K_1 is large, the structural length scales associated with hysteresis and coercivity are much smaller than R_sd.

The critical single-domain radius can also be written as $R_\mathrm{sd} = 36\kappa l_\mathrm{ex}$, where

$$\kappa = \sqrt{\frac{K_1}{\mu_0 M_\mathrm{S}^2}} \tag{10.19}$$

is the magnetic *hardness* parameter and

$$l_\mathrm{ex} = \sqrt{\frac{A}{\mu_0 M_\mathrm{S}^2}} \tag{10.20}$$

is the *exchange length*. The exchange length l_ex is the length below which atomic exchange interactions dominate typical magnetostatic fields. For example, we will see that l_ex determines the coherence radius R_coh below which interatomic exchange is able to ensure coherent rotation. It also determines the thickness of soft-magnetic films below which Néel walls are energetically more favorable than Bloch walls and the grain size of two-phase magnets below which the hysteresis loops look single-phase like.

Table 10.2 shows typical micromagnetic parameters. Note that magnetically very hard and very soft materials are characterized by $\kappa \gg 1$ and $\kappa \ll 1$, respectively, whereas $l_\mathrm{ex} = 3$ nm for a broad range of magnetic materials.

10.3.3 Hysteresis and Coercivity

In order to explain the hysteresis loop of magnetic materials one needs to trace the local magnetization $\boldsymbol{M}(\boldsymbol{r}) = M_\mathrm{S}\boldsymbol{s}(\boldsymbol{r})$ as a function of the applied field H. The starting point is the magnetic energy functional E_m obtained by adding the exchange energy (10.3), the anisotropy energy, the magnetostatic self-energy, as

Table 10.2. Micromagnetic parameters at room temperature. (The values for Fe and Ni are uniaxial estimates).

Material	$\mu_0 M_S$	A	K_1	δ	γ	l_{ex}	κ	R_{sd}	H_0
	T	pJ/m	MJ/m^3	nm	mJ/m^2	nm		nm	T
Fe	2.15	8.3	0.05	40	2.6	1.5	0.12	6	0.06
Co	1.76	10.3	0.53	14	9.3	2.0	0.46	34	0.76
Ni	0.61	3.4	-0.005	82	0.5	3.4	0.13	16	0.03
$BaFe_{12}O_{19}$	0.47	6.1	0.33	14	5.7	5.9	1.37	290	1.8
$SmCo_5$	1.07	22.0	17	3.6	77	4.9	4.35	764	40
$Nd_2Fe_{14}B$	1.61	7.7	4.9	3.9	25	1.9	1.54	107	7.6

implied by (10.17), and the Zeeman energy $-\mu_0 \boldsymbol{M} \cdot \boldsymbol{H} V$ describing the interaction with the applied field. For K_1-only uniaxial magnets we obtain

$$E_m = \int \left[A \left(\frac{\nabla \boldsymbol{M}}{M_S} \right)^2 - K_1 \left(\frac{\boldsymbol{n} \cdot \boldsymbol{M}}{M_S} \right)^2 - \frac{1}{2} \mu_0 \boldsymbol{M} \cdot \boldsymbol{H}_d(\boldsymbol{M}) - \mu_0 \boldsymbol{M} \cdot \boldsymbol{H} \right] \mathrm{d}V \tag{10.21}$$

where $\boldsymbol{n}(\boldsymbol{r})$ is a unit vector denoting the crystallite's easy axis.

As illustrated in Fig. 10.4, hysteresis indicates difficulties in reaching the global (free) energy minimum. As a crude rule – and aside from the Stoner–Wohlfarth-like reversal in weakly interacting particle ensembles – there are two main coercivity mechanisms: nucleation and pinning. *Nucleation* determines the coercivity of nearly homogeneous magnets and means that the magnetization reversal occurs immediately after the original magnetization state becomes unstable. Examples are the Stoner–Wohlfarth nucleation field (10.16), which describes the reversal of the magnetization of an isolated small particle, and the localized nucleation [38] in submicron particles. *Pinning* governs the magnetization reversal in strongly inhomogeneous magnets and means that the coercivity is determined by the interaction of domain walls with structural inhomogenities. To realize magnetization reversal in pinning-controlled magnets, the reverse external field must be larger than some (de)pinning (or propagation) field. One typical pinning mechanism involves inhomogenities whose anisotropy constant is higher than that of the main phase: since high anisotropies yield high domain-wall energies, the penetration of the wall into the highly anisotropic regions is energetically unfavorable. This mechanism is also known as repulsive pinning, whereas the capturing of a wall in a low-anisotropy region is referred to as attractive pinning.

The trapping of walls by a small number of powerful pinning centers is called *strong pinning*. A simple strong-pinning expression is $H_p =$

$(\mathrm{d}\gamma(x)/\mathrm{d}x)/(2\mu_0 M_\mathrm{S})$, where $\gamma(x)$ is the average wall energy as a function of the wall position [14,36]. By contrast, pinning caused by a large number of very small pinning centers, such as atomic defects, is called *weak pinning*. In the case of weak pinning, the wall energy is averaged over a distance of order δ_B, so that the density of pinning centers determines the pinning strength. Another mechanism involves many nucleation centers, so that the magnetization reversal is realized by the pinning-controlled growth and coalescence of a large number of domains.

In the hysteresis loop, the difference between nucleation and pinning is seen most easily from the virgin curves, which are obtained by thermal demagnetization. Figure 10.8 illustrates this distinction. After thermal demagnetization, domain walls in nucleation-controlled particles are very mobile, so that saturation is achieved in very low fields. By contrast, pinning centers impede the domain wall motion in both the virgin-curve and major-loop regimes.

For structurally (morphologically) homogeneous ellipsoids of revolution having the easy axis parallel to the axis of revolution, the nucleation problem can be solved exactly [12,13,14]. This is of some practical importance, because acicular (wire- or needle-like) magnets, fine particles, and thin films can be approximated by prolate, spherical, or oblate ellipsoids of revolution. The calculation consists of two steps: (i) the linearization of (10.21), as discussed in Sect. 10.4, and (ii) solving the resulting stability problem by eigenmode analysis. The corresponding eigenmodes $\boldsymbol{m}(\boldsymbol{r}) = \boldsymbol{M}(\boldsymbol{r}) - M_\mathrm{S}\boldsymbol{e}_z$ are known as *nucleation modes*, and the

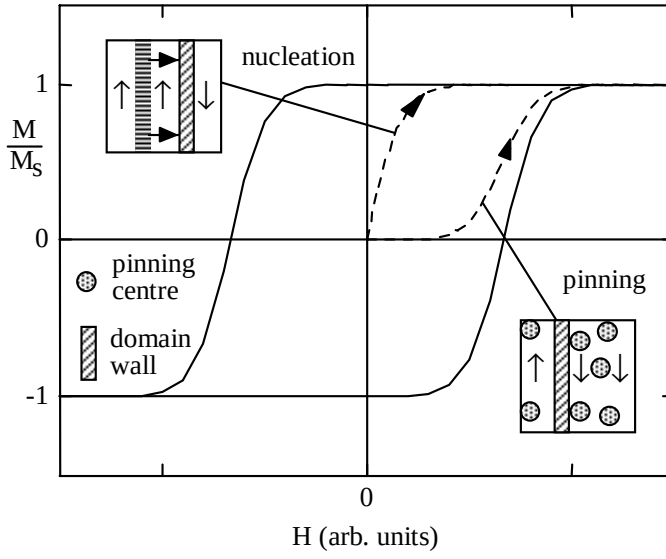

Fig. 10.8. Virgin curves for pinning-controlled and nucleation-controlled permanent magnets.

field at which the instability of the $\boldsymbol{m}(\boldsymbol{r}) = 0$ state occurs is the nucleation field.

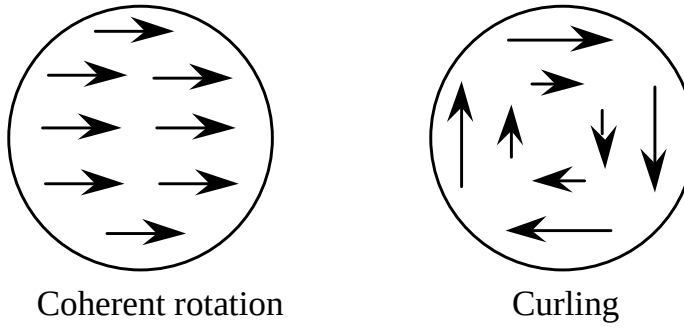

Fig. 10.9. Nucleation modes in homogeneous ellipsoids of revolution (top view on the equator plane). The arrows show $\boldsymbol{m}(\boldsymbol{r})$.

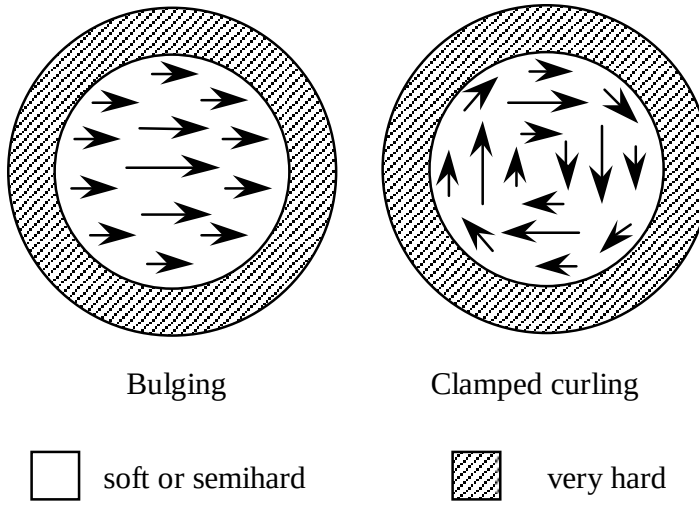

Fig. 10.10. Nucleation modes in spheres surrounded by a hard-magnetic shell (top view on the equator plane). The arrows show $\boldsymbol{m}(\boldsymbol{r})$ for the core phase; in the surrounding shell, $\boldsymbol{m}(\boldsymbol{r}) = 0$. In both cases, the radial dependence of $\boldsymbol{m}$ is given by spherical Bessel functions and localized in the soft region.

The nucleation field is [13,14]

$$H_{\mathrm{N}} = \frac{2K_1}{\mu_0 M_{\mathrm{S}}} + \frac{1}{2}(1 - 3N)\, M_{\mathrm{S}} \tag{10.22}$$

for coherent rotation and

$$H_{\mathrm{N}} = \frac{2K_1}{\mu_0 M_{\mathrm{S}}} - NM_{\mathrm{S}} + \frac{cA}{\mu_0 M_{\mathrm{S}} R^2} \tag{10.23}$$

for the so-called curling mode. Here the radius $R = R_x = R_y$ refers to the two degenerate axes of the ellipsoid, and $c = 8.666$ for spheres ($N = 1/3$) and $c = 6.678$ for needles ($N = 0$). Coherent rotation and curling are realized in small magnets ($R < R_{\mathrm{coh}}$) and large magnets ($R > R_{\mathrm{coh}}$), respectively, where the coherence radius R_{coh} is of the order of $5l_{\mathrm{ex}}$ [37]. Note that these radii are *independent* of K_1. Figure 10.9 compares the coherent-rotation and curling modes. Coherent rotation is favorable from the point of view of exchange, but the exchange energy necessary to realize curling competes with the gain in magnetostatic energy associated with the flux-closure clearly visible in Fig. 10.10. We also deduce that the flux-closure contribution dominates the exchange in large magnets.

The coherent-rotation and curling modes are delocalized, that is the nucleation mode extends throughout the magnet. In general, inhomogenities lead to a localization of the nucleation mode [38]. An exactly solvable case is a soft or semi-hard magnetic sphere surrounded by a hard-magnetic shell. Eigenmode analysis then yields a *bulging* mode characterized by the symmetry of the coherent-rotation mode but incoherent due to the radial dependence of $\boldsymbol{m}$ [39].

Figure 10.10 compares the bulging mode, realized for small particles, with the corresponding modified curling mode realized in large particles. The ultimate reason for the incoherent character of the bulging mode are the boundary conditions at the interface between the two magnetic phases. This yields not only an increase of the nucleation-field coercivity, as compared to Fig. 10.9, but also a singularity at the interface. In Sect. 10.4 we will see under which circumstances grain boundaries are sources of magnetoresistance.

10.3.4 Time Dependence of Magnetic Properties

The non-equilibrium character of magnetization processes means that magnetic properties are time-dependent. There are two basic types of time-dependent magnetic phenomena. Fast atomic processes lead to equilibrium on a local scale and realize intrinsic properties on sub-nanosecond time scales. For this reason, intrinsic properties can be regarded as equilibrium properties, and the energy functional (10.21) is also known as the micromagnetic *free* energy. Micro-magnetic processes are much slower, because atomic thermal excitations have to compete against many-atom energy barriers. For example, permanent magnetism relies on the fact that typical energy barriers are much larger than $\mathrm{k_B}T$ [14]. Intermediate time scales are used, for example, to explain phenomena such as spin-wave resonance (see Chap. 15).

In a strict sense, ferromagnetism is limited to infinite magnets, because thermal excitations in finite magnets cause the net moment to fluctuate between opposite directions and yield – ultimately – a zero spontaneous magnetization. However, the corresponding equilibration time may be very large, and in practice it is often difficult to distinguish the magnetism of small particles from true ferromagnetism. In structurally inhomogeneous magnets (two-phase magnetism), each non-equivalent site i exhibits a local spontaneous magnetization $M_i(T)$, and there is only one common Curie temperature. However, when the size of the

inhomogenities is larger than about 1 nm, it is quite difficult to distinguish the inhomogeneous ferromagnet from a mixture of two phases [40].

A manifestation of *extrinsic* dynamics is that freshly magnetized permanent magnets loose a small fraction of their magnetization within the first few hours, which is known as *magnetic viscosity*. Typically, the magnetization loss is logarithmic, $\Delta M = -S\ln(t)$, where S is the magnetic-viscosity constant [14,36,41]. A related effect is that coercivity depends on the sweep rate $\mathrm{d}H/\mathrm{d}t$ used to measure the loops: H_c is largest for high sweep rates, that is for fast hysteresis-loop measurements.

Small energy barriers, realized for example in fine-particle ensembles, give rise to *superparamagnetism*. First, in particles whose radius is smaller than about 1 nm the external magnetic field is unable to produce saturation, because it cannot compete against thermal excitations. Secondly, there is a blocking radius below which thermal excitations are able to overcome anisotropy-energy barriers. Blocking radii scale as $(T/K_1)^{1/3}$ and are of the order of 5 nm for semi-hard materials.

10.4 Grain–boundary Magnetism

Real polycrystalline (nanocrystalline) magnets exhibit intergranular exchange coupling and magnetostatic interactions between grains. Strong intergranular interactions lead to the breakdown of the picture of individual grains and the magnetic reversal becomes a cooperative effect involving many grains.

A simple model is the *Preisach model*, where the interactions appear as random magnetic fields acting on the individual crystallites [36], but internal interaction fields are unable to give an appropriate description of cooperative magnetization processes. In fact, the validity of the internal-field approach is restricted to the non-cooperative ensembles, where the width of the switching-field distribution $P(H_\mathrm{c})$ of the (non-interacting) crystallites is larger than the magnitude of the interaction fields [42].

A better approach is the *random-anisotropy* theory [43,44,45,46], which focuses on the competition between interatomic exchange and random anisotropy. There are two main random-anisotropy effects: (i) the exchange favors parallel spin alignment throughout the magnet, and the remanence is exchanged-enhanced and (ii) in the limit of strong exchange interactions the coercivity of isotropic magnets vanishes. The relative strength of the intergranular exchange can be expressed in terms of the dimensionless parameter A/K_1R^2, where R is an average grain radius. This parameter shows that intergranular exchange is most effective in the limit of small grain sizes.

However, the original random-anisotropy theory cannot be used when two or more structural length scales are involved. This refers in particular to the effect of sharp grain boundaries [42,47]. Here we present a linear grain-boundary theory, which applies to weakly misaligned grains and is compatible with the scattering mechanism mentioned in the introduction.

10.4.1 Model

Consider an ensemble of exchange-coupled misaligned grains characterized by the local exchange stiffness $A(\boldsymbol{r})$ and the local easy direction $\boldsymbol{n}(\boldsymbol{r})$. The starting point of the calculation is (10.21). Since SMR scales as $(\nabla \boldsymbol{M})^2$, we can restrict ourselves to short length scales, where magnetostatic interactions are of secondary importance (Sect. 10.3.2), and incorporate the self-interaction field into $\boldsymbol{H}$. To linearize the problem we consider weakly misaligned grains and small deviations from perfect spin alignment. Since $|\boldsymbol{M}(\boldsymbol{r})| = M_\mathrm{S}$ and $|\boldsymbol{n}(\boldsymbol{r})| = 1$, we can then write

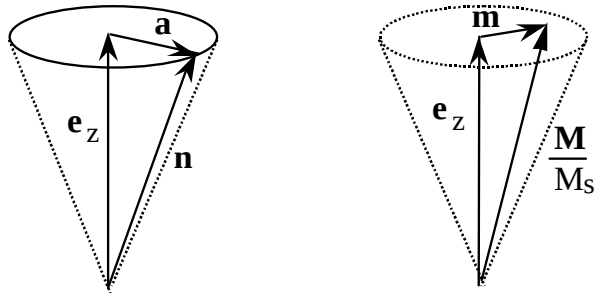

Fig. 10.11. Unit vectors $\boldsymbol{n}(\boldsymbol{r})$ and $\boldsymbol{M}(\boldsymbol{r})/M_\mathrm{S}$ describing the polycrystalline easy axes and the local magnetization, respectively.

$$\boldsymbol{n}(\boldsymbol{r}) = \left(1 - \frac{\boldsymbol{a}(\boldsymbol{r})^2}{2}\right) \boldsymbol{e}_z + \boldsymbol{a}(\boldsymbol{r}) \tag{10.24}$$

and

$$\boldsymbol{M}(\boldsymbol{r}) = M_\mathrm{S} \left(1 - \frac{\boldsymbol{m}(\boldsymbol{r})^2}{2}\right) \boldsymbol{e}_z + M_\mathrm{S} \boldsymbol{m}(\boldsymbol{r})\,, \tag{10.25}$$

where $a \ll 1$, $m \ll 1$, abd $\boldsymbol{a} \cdot \boldsymbol{e}_z = \boldsymbol{m} \cdot \boldsymbol{e}_z = 0$. Figure 10.11 illustrates the meaning of $\boldsymbol{a}$ and $\boldsymbol{m}$.

Putting (10.24), (10.25) into (10.21) and taking $\boldsymbol{H} = -H\boldsymbol{e}_z$ yields

$$E = \int \left[A(\boldsymbol{r}) \left(\nabla \boldsymbol{m}\right)^2 + K_1 \left(\boldsymbol{m} - \boldsymbol{a}(\boldsymbol{r})\right)^2 - \frac{\mu_0 M_\mathrm{S} H}{2} \boldsymbol{m}^2\right] \mathrm{d}V\,. \tag{10.26}$$

Minimizing this equation with respect to $\boldsymbol{m}$ we obtain

$$-\nabla \left(A(\boldsymbol{r}) \nabla \cdot \boldsymbol{m}\right) + \left(K_1 - \mu_0 M_\mathrm{S} H/2\right) \boldsymbol{m} = K_1 \boldsymbol{a}\,. \tag{10.27}$$

Next we consider a grain boundary in the y-z-plane, as shown in Fig. 10.12. This is reasonable, because the perturbation $m(x)$ caused by the grain boundaries decays quite fast in the interior of the grains [42]. Since $\boldsymbol{a} = a\boldsymbol{e}_y$ and

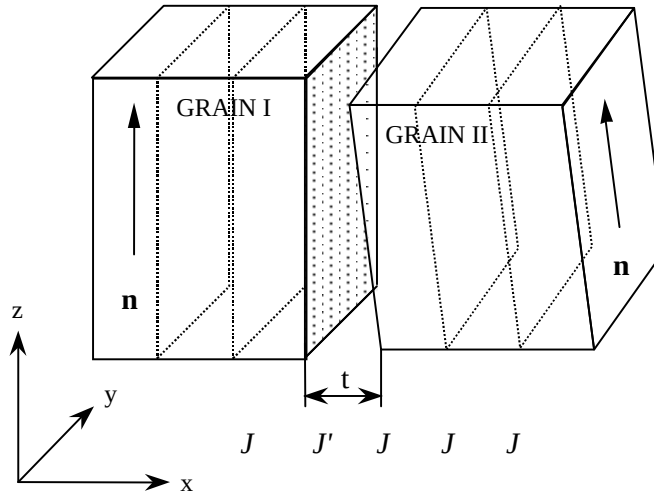

Fig. 10.12. Two neighboring grains and grain boundary. In this section, both continuum and layer-resolved configurations are discussed.

$\boldsymbol{m} = m\boldsymbol{e}_y$, (10.27) now simplifies to

$$-\frac{\partial}{\partial x}\left[A(x)\,\frac{\partial m}{\partial x}\right] + \left[K_1 - \frac{\mu_0 M_\mathrm{S} H}{2}\right] m = K_1 a(x) \tag{10.28}$$

where $a(x)$ is equal to a_I and a_{II} in the respective grains I and II.

10.4.2 Boundary Conditions

As one can see from Fig. 10.10, grain or phase boundaries lead to singularities in the magnetization ($\boldsymbol{M}$ or $\boldsymbol{m}$) and may be potential sources of a pronounced magnetoresistance. The boundary conditions implied by (10.27) and (10.28) have been discussed in [48]. For an interface located at x_0, integration from $x_0 - \varepsilon$ to $x_0 + \varepsilon$ yields

$$\left[A(x)\,\frac{\partial m}{\partial x}\right]_{x_0-\varepsilon} = \left[A(x)\,\frac{\partial m}{\partial x}\right]_{x_0+\varepsilon}. \tag{10.29}$$

This means that a jump in $A(\boldsymbol{r})$ changes the *slope* of the perpendicular magnetization component m.

Figure 10.13 shows that the boundary conditions (10.29) give rise to a variety of scenarios. In Fig. 10.13a, a phase I characterized by a large exchange stiffness is coupled to a phase II having a low A. When the anisotropy of phase I is very high, then the mode $\boldsymbol{m}(\boldsymbol{r})$ is localized in the phase II characterized by low or moderate anisotropy, regardless of the value of A in the two phases. This regime is illustrated in Fig. 10.13b and realized, for example, in the composite Fig. 10.10. Of particular interest in spin electronics is the case where two grains

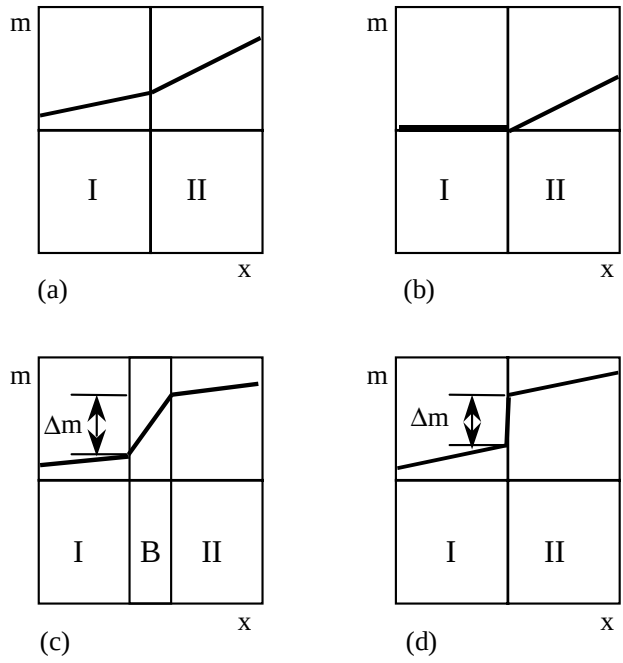

Fig. 10.13. Boundary conditions at interfaces: (a) interface between two phases of different exchange stiffness, (b) interface between hard and soft regions, (c) effect of grain-boundary region characterized by reduced exchange, and (d) reduced exchange coupling at interface. Note that (d) may be interpreted as a special case of (c) where $B = 0$.

are separated by a grain-boundary region (B) of reduced exchange stiffness. As shown in Figs. 10.13c and d, this leads to a *quasi-discontinuity* Δm of the magnetization with a strong potential for SMR.

In order to calculate the magnitude of the quasi-discontinuity, we assume a thin grain-boundary region of thickness t whose exchange stiffness A' is smaller than the bulk exchange stiffness A (Fig. 10.13c). Putting, for simplicity, $H = 0$ in (10.28) [49], we see that $m = a$ well inside the grains. It is therefore useful to consider the quantity $\Delta = \Delta m/|a_{II} - a_I|$, that is the fraction of the magnetization variation concentrated in the grain-boundary region. In the bulk, the difference $m-a$ decays exponentially [42], so that the calculation of Δ amounts to incorporating the boundary condition (10.29). After short calculation we obtain

$$\Delta = \frac{1}{1 + \frac{2A'\delta}{\pi A t}} \,. \tag{10.30}$$

For $t = 0$, the quasi-discontinuity vanishes ($\Delta = 0$), whereas zero intergranular exchange ($A' = 0$) leads to $\Delta = 1$. On the other hand, since t tends to

be much smaller than the wall width δ, an exchange enhancement at the grain boundary ($A' > A$) has no major impact on Δ.

10.4.3 Layer–Resolved Spin Structure

Equation (10.28) describes ferromagnets on a continuum level, so that magnetization processes cannot be resolved on an atomic scale. For example, as indicated in Fig. 10.13d, grain boundaries tend to be atomically thin, and it is difficult to judge whether (10.30) remains valid in this limit.

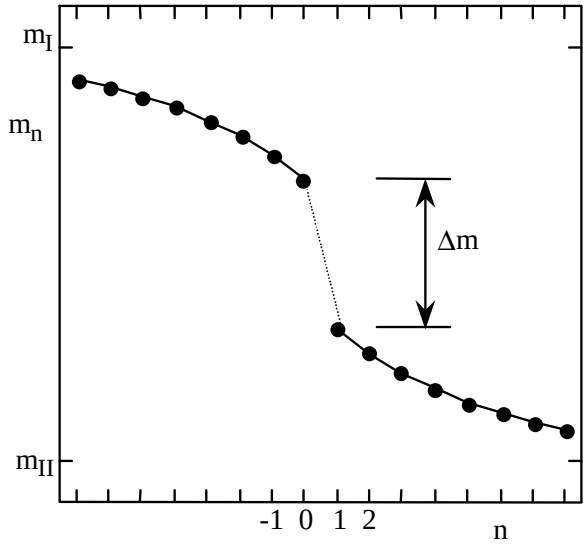

Fig. 10.14. Spin structure in the vicinity of the grain boundary. The jump Δm means a quasi-discontinuity of the magnetization at the grain boundary.

In a layer-resolved analysis, as envisaged in Fig. 10.12, (10.28) must be replaced by

$$E = \sum_{n=-\infty}^{\infty} \left[J_{n,n+1} \frac{(\boldsymbol{M}_n - \boldsymbol{M}_{n+1})^2}{M_S^2} - K_1 S_0 t_0 \frac{(\boldsymbol{n}_n \cdot \boldsymbol{M}_n)^2}{M_S^2} - \mu_0 \boldsymbol{M}_n \cdot \boldsymbol{H} S_0 t_0 \right] \tag{10.31}$$

where S_0 is the interface area, $J_{n,n+1} \simeq A(\boldsymbol{r})t_0$ is the interlayer exchange coupling between adjacent atoms in the n-th and (n+1)-th layers, and each layer (index n) has a thickness $t_0 = t$. Restricting ourselves to the remanent state ($H = 0$) and using the approximation (10.25) we obtain, aside from a physically irrelevant zero-point energy,

$$E = \sum_{n=-\infty}^{\infty} \left[J_{n,n+1}(m_n - m_{n+1})^2 + K_1 S_0 t_0 (m_n - a_n)^2 \right] . \tag{10.32}$$

Here the interatomic *interface exchange* $J_{0,1} = J'$ is smaller than the bulk exchange $J_{n,n+1} = J$ for $n \neq 0$ (Fig. 10.12). Minimizing (10.32) yields the set of equations

$$J_{n,n+1}(m_n - m_{n+1}) + K_1 S_0 t_0 m_n = K_1 S_0 t_0 a_n \tag{10.33}$$

subject to the boundary conditions $m_n = a_{I/II}$ for $n = \pm\infty$.

A typical solution is shown in Fig. 10.14. For $n < 0$ and $n > 1$, the dependence of the layer-resolved perpendicular magnetization contribution m_n on n is exponential, $(m_n - a_{I/II}) \sim \exp(\pm n/\lambda)$, and the decay length is

$$\lambda = \frac{1}{\operatorname{arcosh}(1 + K_1 S_0 t_0 / 2J)} \tag{10.34}$$

In the interesting limit $K_1 S_0 t_0 \ll J$ this reduces to the bulk-type wall-width expression $(J/K_1 S_0 t_0)^{1/2}$. As in the continuum limit, the reduced interface exchange yields a quasi-discontinuity $\Delta m = m_1 - m_0$. For $K_1 S_0 t_0 \ll J$, we obtain

$$\Delta = \frac{\sqrt{K_1 S_0 t_0 J}}{\sqrt{K_1 S_0 t_0 J} + 2J'} \,. \tag{10.35}$$

Aside from the use of atomic parameters, this result is very similar to (10.30).

Due to the quadratic dependence of SMR on the magnetization gradient, most of the magnetoresistive scattering by weakly coupled grains is associated with the quasi-discontinuity Δ. From (10.30) and (10.35) we deduce that $\Delta = 1$ for $A' = 0$ and $J' = 0$, respectively, that is for zero intergranular exchange. Compared to ordinary domain-wall scattering, this corresponds to an increase of the magnetoresistance by a factor of order δ/t_0, that is of the order of 100 for many materials of interest in spin electronics. However, a comparatively weak intergranular exchange is sufficient to yield a strong reduction of Δ. Taking $t = t_0$ (one layer of reduced exchange) we find that $\Delta = 1/2$ when A'/A and J'/J are about t_0/δ, that is of the order of 0.01. This means that SMR materials are not very forgiving with respect to residual intergranular exchange.

10.5 Concluding Remarks

A key finding of this chapter is that reduced exchange at grain boundaries yields a quasi-discontinuity of the magnetization, corresponding to a disproportionally strong domain-wall type magneto-resistance. By comparison, enhanced exchange in a thin grain-boundary region has no major effect on the spin structure. The same is true for anisotropy changes in the grain-boundary region, because the effect of anisotropy inhomogenities averages over at least a few nm.

The atomic origin of the grain-boundary exchange is of secondary importance in micromagnetism, because it is treated as a parameter. In any case, there is no conduction without some rudimentary exchange, so that the intergranular exchange may be small but is always nonzero.

The results obtained in Sect. 10.4 do not depend very much on whether one uses continuum or layer-resolved models. However, this does not mean that the

relation between intrinsic and extrinsic properties at grain-boundaries is trivial, and a thorough and comprehensive description of the magnetic and magnetoresistive phenomena at grain boundaries remains a challenge.

Since the wall-width parameter δ scales as $(A/K_1)^{1/2}$, the domain-wall scattering is particularly strong in hard magnets, but in that case one needs undesirably large magnetic fields to change the spin configuration. Reduced intergranular exchange has a much more favorable effect on the magnetoresistance. From the point of view of spin-projecting magnetoresistance (SMR), the ideal magnetoresistive material is a hard-soft nanocomposite characterized by very weak intergranular exchange [50]. Of course, the realization of such a material remains a real challenge to atomic theory and magnet processing.

Note, finally, that SMR requirements are similar to the situation encountered in magnetic recording, where pronounced intergranular exchange between semi-hard grains leads to 'interaction domains' and reduces the storage density [51]. By contrast, two-phase permanent magnetism relies on a strong exchange coupling between hard and soft regions [42].

Acknowledgement

Thanks are due to Prof. D. J. Sellmyer for discussing the manuscript. This work was supported by DOD, DOE, OXSEN, and CMRA.

References

1. M. N. Baibich, J. M. Broto, A. Fert, F. Nguyen Van Dau, F. Petroff, P. Etienne, G. Creuzet, A. Friederich, and J. Chazelas, Phys. Rev. Lett. **61**, 2472 (1988).
2. A. E. Berkowitz, J. R. Mitchell, M. J. Carey, A. P. Young, S. Zhang, F. E. Spada, F. T. Parker, A. Hutten, and G. Thomas, Phys. Rev. Lett. **68**, 3745 (1992).
3. J. Q. Xiao, J. S. Jiang, and C. L. Chien, Phys. Rev. Lett. **68**, 3749 (1992).
4. J. F. Gregg, W. Allen, K. Ounadjela, M. Viret, M. Hehn, S. M. Thompson, and J. M. D. Coey, Phys. Rev. Lett. **77**, 1580 (1996).
5. P. M. Levy and S. Zhang, Phys. Rev. Lett. **79**, 5110 (1997).
6. R. von Helmolt, J. Wecker, B. Holzapfel, L. Schultz, and K. Samwer, Phys. Rev. Lett. **71**, 2331 (1993).
7. J. M. D. Coey, M. Viret, L. Ranno, and K. Ounadjela, Phys. Rev. Lett. **75**, 3910 (1995).
8. P. Schiffer, A. P. Ramirez, W. Bao, and S.-W, Cheong, Phys. Rev. Lett. **75**, 3339 (1995).
9. N. D. Mathur, G. Burnell, S. P. Isaac, T. J. Jackson, B.-S. Theo, J. L. MacManus Driscoll, L. F. Cohen, J. E. Evetts, and M. G. Blamire, Nature **387**, 266 (1997).
10. J. M. D. Coey, A. E. Berkowitz, Ll. Balcells, F. F. Putris, and A. Barry, Phys. Rev. Lett. **80**, 3815 (1998).
11. N. F. Mott and H. Jones, "The Theory of the Properties of Metals and Alloys", (University Press, Oxford, 1936).
12. W. F. Brown, "Micromagnetics", (Wiley, New York, 1963).
13. A. Aharoni, "Introduction to the Theory of Ferromagnetism", (University Press, Oxford, 1996).

14. R. Skomski and J. M. D. Coey, "Permanent Magnetism", (Institute of Physics, Bristol, 1999).
15. H. R. Hilzinger and H. Kronmüller, Phys. Lett. **51A** 59 (1975).
16. M. Viret, D. Vignoles, D. Cole, J. M. D. Coey, W. Allen, D. S. Daniel, and J. F. Gregg, Phys. Rev. B **53**, 8464 (1996).
17. A. Gupta, G. Q. Gong, G. Xiao, P. R. Duncombe, P. Lecoeur, P. Trouilloud, Y. Y. Wang and V. P. Dravid, and J. Z. Sun, Phys. Rev. B **54**, 15629 (1996).
18. E. Ising, Z. Phys. **31**, 253 (1925).
19. W. Heisenberg, Z. Phys. **49**, 619 (1928).
20. F. Bloch, Z. Phys. **57**, 545 (1929).
21. H. Brooks, Phys. Rev. **58**, 909 (1940).
22. J. C. Slater, Rev. Mod. Phys. **25**, 199 (1953).
23. F. Bloch, Z. Phys. **74**, 295 (1932).
24. L. Landau and E. Lifshitz, Phys. Z. Sowjetunion **8**, 153 (1935).
25. M. Kersten, Z. Phys. **44**, 63 (1943).
26. F. Cyrot-Lackmann, J. Phys. Chem. Solids **29**, 1235 (1968).
27. A well-known exception is, for example, the 'very weak intinerant ferromagnet' $ZrZn_2$.
28. Note that first, second, and third anisotropy constants, respectively, correspond to – at least – second-, fourth-, and sixth-order anisotropy contributions [14].
29. R. Skomski, H.-P. Oepen, and J. Kirschner, Phys. Rev. B **58**, 11138 (1998).
30. F. Bloch and G. Gentile, Z. Phys. **70**, 395 (1931).
31. E. C. Stoner and E. P. Wohlfarth, Phil. Trans. Roy. Soc. **A240**, 599 (1948).
32. In this equation, the factor 1/2 is necessary to avoid double-counting interacting pairs of atomic moments.
33. C. Kittel, Rev. Mod. Phys. **21**, 541 (1949).
34. D. J. Craik and R. S. Tebble, Rep. Prog. Phys. **24** 116 (1961).
35. S. Chikazumi, "Physics of Magnetism", (Wiley, New York, 1964).
36. R. Becker and W. Döring, "Ferromagnetismus", (Springer, Berlin, 1939).
37. The coherence radius $R_{\rm coh}$ is obtained by equating (10.22) and (10.23). Note that $R_{\rm coh}$ is independent of K_1.
38. R. Skomski, J. Appl. Phys. **83**, 6503 (1998).
39. R. Skomski, J. P. Liu, and D. J. Sellmyer, Phys. Rev. B **60**, 7359 (1999).
40. R. Skomski and D. J. Sellmyer, J. Appl. Phys. **87**, 4756 (2000).
41. E. Kneller, "Ferromagnetismus" (Springer, Berlin, 1962).
42. R. Skomski, J. P. Liu, J. M. Meldrim, and D. J. Sellmyer, in "Magnetic Anisotropy and Coercivity in Rare-Earth Transition Metal Alloys", eds., L. Schultz and K.-H. Müller, (Werkstoffinformationsgesellschaft, Frankfurt/M., 1998), p. 277.
43. R. Harris, M. Plischke, and M. J. Zuckermann, Phys. Rev. Lett. **31**, 160 (1973).
44. K. Moorjani and J. M. D. Coey, "Magnetic Glasses", (Elsevier, Amsterdam, 1984).
45. E. M. Chudnovsky, W. M. Saslow, and R. A. Serota, Phys. Rev. B **33**, 251 (1986).
46. R. Skomski, J. Magn. Magn. Mater. **157-158**, 713 (1996).
47. T. Schrefl and J. Fidler, J. Magn. Magn. Mater. **175-181**, 970 (1998).
48. R. Skomski and J. M. D. Coey, Phys. Rev. B **48**, 15812 (1993).
49. Positive and negative fields reduce and enhance the spin inhomogenity, respectively, but a detailed analysis of the field dependence goes beyond this work.
50. The hard phase, which does not switch in small fields, could be ferrimagnetic to reduce the magnetostatic interactions between the grains.
51. D. J. Sellmyer, M. Yu, R. A. Thomas, Y. Liu, and R. D. Kirby, Phys. Low-Dim. Struct. **1-2**, 153 (1997).